Available online at www.sciencedirect.com
SCIENCE DIRECT®
Journal of Solid State Chemistry 177 (2004) 332–342
JOURNAL OF SOLID STATE CHEMISTRY
http://elsevier.com/locate/jssc

Synthesis of a new donor, BEDT-HBDST and crystal structures, electrical and magnetic properties of (BEDT-HBDST)$_2MX_4$ (M = Fe, Ga, X = Cl, Br), where BEDT-HBDST = 2,5-bis(4,5-ethylenedithio-1,3-diselenol-2-ylidene)-2,3,4,5-tetrahydrothiophene

Takashi Shirahata,[a,b] Takehiko Mori,[c] and Kazuko Takahashi[d,*]

[a] Department of Chemistry, Graduate School of Science, Tohoku University, Sendai 980-8578, Japan
[b] The Institute of Physical and Chemical Research (RIKEN), Wako, Saitama 351-0198, Japan
[c] Department of Organic and Polymeric Materials, Tokyo Institute of Technology, O-okayama, Tokyo 152-8552, Japan
[d] Center for Interdisciplinary Research, Tohoku University, Sendai 980-8578, Japan

Received 7 May 2003; received in revised form 11 August 2003; accepted 21 August 2003

Abstract

A novel conjugation-elongated bis(ethylenedithio)tetraselenafulvalene (BETS) type donor, 2,5-bis(4,5-ethylenedithio-1,3-diselenol-2-ylidene)-2,3,4,5-tetrahydrothiophene (BEDT-HBDST) and its magnetic and non-magnetic anion salts, (BEDT-HBDST)$_2MX_4$ (MX_4^- = $FeCl_4^-$, $GaCl_4^-$, $FeBr_4^-$ and $GaBr_4^-$), were prepared. These four salts are isostructural and belong to the space group of $P2/c$. They showed semiconducting behavior with small activation energies (59–64 meV). The band structures of these salts are quasi one-dimensional and there is a midgap between the upper band and the lower band, since the degree of dimerization is significant in the stacking direction. The MX_4^- ions are located between the donor columns and near to the ethylenedithio moieties of the donor molecules. The magnetic susceptibilities of the $FeCl_4^-$ and $FeBr_4^-$ salts follow the Curie–Weiss law with Curie constants of 4.6 and 4.8 emu K mol^{-1} (sum of the spins of $S = 5/2$ and $S = 1/2$) and negative Weiss temperatures of $\theta = -1.2$ and -4.9 K, respectively, revealing a weak antiferromagnetic interaction of 3d spins of the $FeCl_4^-$ and $FeBr_4^-$ anions. The Fe···Fe (6.66–7.60 Å), Cl···Cl (4.81–4.82 Å) and Br···Br (4.74–4.77 Å) distances in the crystal structures of these salts are significantly long. Therefore, the direct magnetic interaction between the 3d spins of the nearest neighboring Fe^{3+} ions appears to be not readily accessible.

Keywords: π-extended donor; BEDT-HBDST; Cation radical salts; Magnetic anions; X-ray structure analysis; Band calculation; Electrical conductivity; π–d system

1. Introduction

For more than 15 years, many efforts have been continued to explore novel multi-functional molecular systems, such as molecular based magnetic conductors in which conducting electrons in donor layers and localized d-spins in the magnetic anion layer are interacting with each other [1]. An example of the strong π–d coupled molecular conductor is Cu–DCNQI system (dicyanoquinonediimine (DCNQI)). In this system, the mixed valence of the copper atom ($Cu^{1.3+}$) forms a π–d mixed metallic band [2]. The first donor-based conductor exhibiting stable metallic behavior and taking place a weak ferromagnetic interaction between Cu^{2+} ions was discovered for (BEDT-TTF)$_3$CuCl$_4$H$_2$O where BEDT-TTF = bis(ethylenedithio)tetrathiafulvalene [3]. The first paramagnetic organic superconductor was discovered for β''-(BEDT-TTF)$_4$(H$_3$O)[Fe(C$_2$O$_4$)$_3$]·PhCN [4]. These early studies were followed by the active investigations on the bis(ethylenedithio)tetraselenafulvalene (BETS)-based salts incorporating Fe^{3+} ions. For example, it was found that λ-(BETS)$_2$FeCl$_4$ undergoes a sharp metal–insulator transition at 8.5 K,

*Corresponding author. Center for Interdisciplinary Research, Tohoku University, Aramaki, Aoba 980-8577, Japan. Fax: +81-22-217-7810.
E-mail address: tkazuko@cir.tohoku.ac.jp (K. Takahashi).

0022-4596/$ - see front matter © 2003 Elsevier Inc. All rights reserved.
doi:10.1016/j.jssc.2003.08.030

where the insulating phase is a π–d coupled antiferromagnetic phase [5]. For the π–d coupling in λ-$(BETS)_2FeCl_4$, the close Se···Cl contacts in the crystal structure play an important role. More recently, weak π–d interactions were found in κ-$(BETS)_2FeBr_4$ and in κ-$(BETS)_2FeCl_4$ in which antiferromagnetic superconducting transitions have been observed [6]. Considering these excellent properties of BETS-based magnetic anion salts, a novel conjugation-elongated BETS-type donor, 2,5-bis(4,5-ethylenedithio-1,3-diselenol-2-ylidene)-2,3,4,5-tetrahydrothiophene (BEDT-HBDST: **1**), incorporating a dihydrothiophene spacer group and four inner selenium atoms appears to be a promising candidate for the donor component of the magnetic anion salts for developing the π–d interaction. Moreover, the four inner Se atoms with large 4pπ orbitals will be quite suitable to induce a good transverse intermolecular orbital overlap and producing a wide bandwidth.

Although many conjugation-elongated tetrathiafulvalene (TTF)- and BEDT-TTF-type donors have been synthesized [7], conjugation-elongated BETS-type donors have not been known so far. Then, we have now designed and synthesized BEDT-HBDST (**1**), and clarified the crystal structure, and electrical and magnetic properties of magnetic anion salts of **1**, such as $(BEDT\text{-}HBDST)_2FeCl_4$ and $(BEDT\text{-}HBDST)_2FeBr_4$, as well as non-magnetic anion salts $(BEDT\text{-}HBDST)_2GaCl_4$ and $(BEDT\text{-}HBDST)_2GaBr_4$ for reference compounds to investigate the possibility of the π–d interaction in these magnetic anion salts.

2. Experimental

2.1. Synthesis

BEDT-HBDST (**1**) was synthesized conveniently according to the route shown in Scheme 1. Succinic thioanhydride (**2**) [8] and 4,5-ethylenedithio-1,3-diselenol-2-one (**3**) [9] were synthesized according to the literature procedures. All reactions were carried out under argon atmosphere. All chemicals and solvents

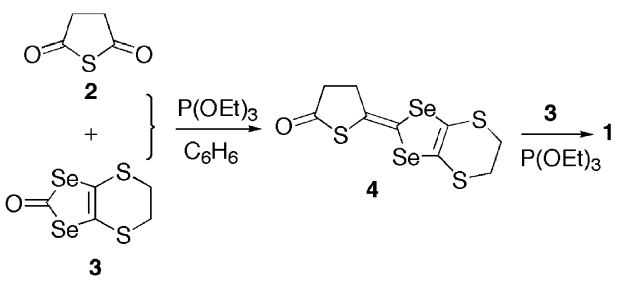

Scheme 1. Synthesis of BEDT-HBDST.

(reagent grade) were dried well and the solvents were distilled before use. Column chromatography was carried out with silica gel (150–425 μm). Melting points were determined with a Yanagimoto micro melting point apparatus MP-J3 and were uncorrected. Elemental analyses were performed at Instrumental Analysis Center for Chemistry, Tohoku University. ^1H NMR spectra were recorded on a Bruker AC-200P spectrometer and chemical shifts are recorded in δ relative to tetramethylsilane as an internal standard. FT-IR spectra were recorded on a HORIBA FT-300 spectrometer with a KBr disk method. Mass spectra were recorded on a JEOL HX-100 or a HITACHI M-2500S spectrometer. Electronic absorption spectra were recorded on a HITACHI U-3210 spectrometer.

2.1.1. 5-(4,5-ethylenedithio-1,3-diselenol-2-ylidene)-2,3,4,5-tetrahydrothiophen-2-one (4)

Succinic thioanhydride (**2**) (100 mg, 0.861 mmol) was dissolved in benzene (30 mL). To this were added triethyl phosphite (30 mL, 172 mmol) and 4,5-ethylenedithio-1,3-diselenol-2-one (**3**) (520 mg, 1.72 mmol) and the resulting solution was heated at reflux for 2 h, during which the reaction mixture turned to a brown suspension. After cooling to room temperature, brown precipitates (BETS), the homo-coupling reaction product of **3**, were removed out by filtration and the solvent of the orange filtrate was evaporated under reduced pressure. The residue was washed well successively with methanol and *n*-hexane. The resulting yellow–orange powder was dissolved in toluene and chromatographed on silica gel by eluting with toluene. The eluent showing yellow–orange band on the column was collected, and the solvent was evaporated under reduced pressure to give **4** (170 mg, 0.440 mmol, 51%) as yellow powder which was successively recrystallized from toluene gave a pure sample of **4** as yellow plates; mp 207–209°C (decomp); ^1H NMR ($CDCl_3$, 200 MHz) δ 2.80 (4H, mc, $=CCH_2CH_2C=$) and 3.32 (4H, s, SCH_2CH_2S); IR (KBr) ν 1699, 1421, 1412, 1288, 1261, 1063, 1043, 995, 922, 879, 816 and 746 cm^{-1}; UV–Vis (THF) λ (log ε) 412 (2.72) and 319 (3.78) nm; MS (EI, 70 eV) *m*/*z* (rel. intensity) 390 ($M^+ + 2$, 40), 389 ($M^+ + 1$, 13), 388 (M^+, 100), 387 (M^+–1, 18), 389 (M^+–2, 88), 385 (M^+–3, 30), 384 (M^+–4, 50), 383 (M^+–5, 14), 382 (M^+–6, 21) and 360 (M^+–C_2H_4, 17). Analytical found: C, 28.17; H, 2.38; S, 25.05%; $C_9H_8OS_3Se_2$ requires: C, 27.99; H, 2.09; S, 24.90%.

2.1.2. 2,5-bis(4,5-ethylenedithio-1,3-diselenol-2-ylidene)-2,3,4,5-tetrahydrothiophene (BEDT-HBDST: 1)

To a solution of **4** (116 mg, 0.300 mmol) in triethyl phosphite (25 mL) was added 4,5-ethylenedithio-1,3-diselenol-2-one (**3**) (45 mg, 0.150 mmol) and the resulting solution was heated at 130°C with stirring for 15 min. To this was added the second portion of **3**

(45 mg, 0.150 mmol) after heating at 130°C for 15 min. In the same interval, total six portions of **3** (45 mg, 0.150 mmol in each portion) were added. The reaction mixture was totally heated at 130°C for 135 min, during which the reaction mixture turned to a brown suspension. After cooling to room temperature, the brown powder separated out was collected by filtration and washed successively with methanol and *n*-hexane. The brown powder was dissolved in carbon disulfide and chromatographed on silica gel by eluting with carbon disulfide to give BEDT-HBDST (**1**) (82 mg, 0.125 mmol, 42%) as yellow powder which was recrystallized from toluene to give a pure sample of BEDT-HBDST as yellow needles; mp 261–263°C (decomp); ^{1}H NMR ($CDCl_3$–CS_2, 200 MHz) δ 2.64 (4 H, s, $=CCH_2CH_2C=$) and 3.31 (8H, s, SCH_2CH_2S); IR (KBr) ν 2945, 2914, 2904, 2877, 1583, 1406, 1282, 1257, 1201, 1171, 1130, 1119, 1080, 922, 868, 812 and 723 cm^{-1}; UV–Vis (THF) λ (log ε) 414 (3.17), 316 (sh, 4.22) and 306 (4.32) nm; MS (EI, 70 eV) m/z (rel. intensity) 660 (M^+, 12), 354 (78), 196 (96), 160 (61) and 88 (100). HRMS found: m/z, 659.6203; $C_{14}H_{12}S_5Se_4$ requires: M, 659.6204; Analytical found: C, 25.88; H, 2.02%; $C_{14}H_{12}S_5Se_4$ requires: C, 25.62; H, 1.84%.

2.1.3. Cation radical salts of BEDT-HBDST

Cation radical salts of the novel dihydrothiophene-extended donor, BEDT-HBDST, were obtained by the galvanostatic electrochemical oxidation method under the conditions listed in Table 1. The supporting electrolytes were used in the form of the tetra-*n*-butylammonium or tetraethylammonium salts. A standard H-shaped cell and platinum wire electrodes (1 mm diameter) were employed and a constant current (0.5 μA) was applied for 10–14 days. After the single crystalline cation radical salts were grown on the anode, the crystals were collected by filtration and washed sequentially with ethanol.

2.2. Physical property measurements

The cyclic voltammetry measurements were performed under argon atmosphere at room temperature. The cyclic voltammograms were taken on a BAS CV-50 W. A solution of 10^{-3} M in benzonitrile with 0.1 M tetra-*n*-butylammonium perchlorate (TBAP) as a supporting electrolyte, glassy carbon as a working electrode and platinum wire as a counter electrode were used. Potentials were referenced versus saturated calomel electrode (SCE). Sweep rate was 500 mV s^{-1}.

The DC-resistivities of cation radical salts were measured with the conventional four-probe technique on using YOKOGAWA 7651 programmable direct current source and KEITHLEY 2001 digital multimeter unit. Gold wires (10 or 15 μm diameter) were attached to a sample with carbon paste.

The magnetic property measurements were carried out with a commercial superconducting quantum interference device (SQUID) magnetrometer manufactured by Quantum Design Co., Ltd. (MPMS2 and MPMS-XL) under the range of the magnetic field between 0 and 50 kOe. The SQUID measurements were performed in the range of temperature $2\,K \leqslant T \leqslant 300\,K$. The crystals were attached randomly to the OHP film sheet, which was cut in 4 mm wide, with small amount of vinyl phenolic adhesive GE 7031 (The Nilaco

Table 1
Conditions of electrochemical crystallization, conducting property and IR data of $(BEDT\text{-}HBDST)_2MX_4$ (MX_4^- = $FeCl_4^-$, $GaCl_4^-$, $FeBr_4^-$ and $GaBr_4^-$)

	$(BEDT\text{-}HBDST)_2FeCl_4$	$(BEDT\text{-}HBDST)_2GaCl_4$	$(BEDT\text{-}HBDST)_2FeBr_4$	$(BEDT\text{-}HBDST)_2GaBr_4$
Condition[a]				
T (°C)	20	20	20	20
Solvent	PhCl (10% EtOH)	PhCl (10% EtOH)	CH_2Cl_2 (10% EtOH)	PhCl
BEDT-HBDST	7 mg	5 mg	3 mg	3 mg
Electrolyte	TBA · $FeCl_4$, 99 mg	TBA · $GaCl_4$, 115 mg	TEA · $FeBr_4$, 30 mg	TBA · $GaBr_4$, 32 mg
Period (days)	14	14	14	10
Appearance	Black plate	Black plate	Black plate	Black plate
mp (°C)	179–183	195–199	183–185	201–204
Conducting property[b]				
$\sigma_{r.t.}$ (S cm^{-1})	0.89	1.0	2.2	3.6
E_a (eV)	0.064 (220–300 K)	0.064 (220–300 K)	0.059 (220–300 K)	0.060 (220–300 K)
	0.071 (85–170 K)	0.11 (75–210 K)	0.034 (30–140 K)	0.040 (40–130 K)
IR data[c]				
ν_{CT} (cm^{-1})	3000	3000	2500	2500

[a] A standard H-shaped cell and platinum wire electrodes (1 mm diameter) were employed. PhCl: chlorobenzene; TEA: tetraethylammonium; TBA: tetra-*n*-butylammonium.

[b] Conductivity was measured with four-probe method and gold wires (10 or 15 μm diameter) were attached with carbon paste. These salts undergo a phase transition from one semiconducting state to another semiconducting state at low temperature.

[c] IR data were measured on a KBr disk.

Table 2
Crystal data for cation radical salts of BEDT-HBDST

Compound Formula	(BEDT-HBDST)$_2$FeCl$_4$ $C_{28}H_{24}S_{10}Se_8FeCl_4$	(BEDT-HBDST)$_2$GaCl$_4$ $C_{28}H_{24}S_{10}Se_8GaCl_4$	(BEDT-HBDST)$_2$FeBr$_4$ $C_{28}H_{24}S_{10}Se_8FeBr_4$	(BEDT-HBDST)$_2$GaBr$_4$ $C_{28}H_{24}S_{10}Se_8GaBr_4$
Formula weight	1510.40	1524.27	1688.24	1702.11
T (K)	293	293	293	293
Crystal system	Monoclinic	Monoclinic	Monoclinic	Monoclinic
Space group	$P2/c$ (#13)	$P2/c$ (#13)	$P2/c$ (#13)	$P2/c$ (#13)
a (Å)	22.4327(15)	22.4213(17)	22.772(3)	22.820(3)
b (Å)	6.6586(5)	6.6490(5)	6.6722(8)	6.6771(8)
c (Å)	15.1248(11)	15.0669(12)	15.1955(19)	15.2240(19)
α (deg)	90	90	90	90
β (deg)	103.513(2)	103.587(2)	102.640(3)	102.765(3)
γ (deg)	90	90	90	90
V (Å^3)	2196.7(3)	2183.3(3)	2252.9(5)	2262.3(5)
Z	2	2	2	2
D_c (g cm^{-3})	2.284	2.319	2.489	2.499
Crystal size (mm^3)	$0.30 \times 0.12 \times 0.03$	$0.55 \times 0.25 \times 0.02$	$0.50 \times 0.20 \times 0.02$	$0.50 \times 0.20 \times 0.05$
μ(Mo$K\alpha$) (cm^{-1})	77.15	80.47	108.33	110.63
Reflections collected	15788	15419	15803	15744
θ range for data collection	0.93–28.31°	0.93–28.36°	1.83–28.34°	0.91–28.29°
Independent reflections	5432	5430	5584	5593
R_{int}	0.0442	0.0592	0.0839	0.0927
Max. and min. transmission	0.8015 and 0.2055	0.8556 and 0.0956	0.8125 and 0.0743	0.6077 and 0.0724
Data/restraints/parameters	5432/0/277	5430/0/231	5584/0/286	5593/0/286
$R_1(I > 2\sigma(I))$	0.0531	0.0610	0.0909	0.0788
w$R_2(I > 2\sigma(I))$	0.1350	0.1656	0.2298	0.2079
Goodness-of-fit on F^2	1.098	1.036	1.010	1.006

Corporation). The magnetic susceptibility was corrected for the diamagnetic contributions estimated from the sum of Pascal constants.

The X-ray diffraction experiment for the single crystalline cation radical salts of BEDT-HBDST was performed on a Bruker AXS SMART APEX CCD detector with graphite monochromatized Mo$K\alpha$ radiation ($\lambda = 0.71073$ Å). A semiempirical absorption correction was applied with the program SADABS [10]. The structures were solved by direct methods (SHELXS-97) [11] and refined by full-matrix least-squares (SHELXL-97) [11] fit on F^2. Non-hydrogen atoms were refined anisotropically, and hydrogen atoms were added in calculated positions with fixed isotropic contributions. Occupancies of disordered positions in the cation radical salts of **1** were refined by least-squares methods. Crystal data and other experimental details are summarized in Table 2. Supplementary crystallographic data have been deposited at the Cambridge Crystallographic Data Center, CCDC 208543–208546.

Intermolecular overlap integrals were calculated with the atomic orbital coefficients of the HOMO obtained by the extended Hückel MO calculations [12] with semiempirical parameters for Slater-type atomic orbitals. The transfer integral (t) is approximately in proportion to the overlap integral (S), $t = \varepsilon S$ ($\varepsilon = -10$ eV; ε is a constant with order of the orbital energies of HOMO). The band structures were calculated based on the tight-binding approximation [13].

3. Results and discussion

3.1. Electrochemical properties

The electrochemical oxidation of BEDT-HBDST (**1**) occurred in reversible two-step one-electron process which was demonstrated in the cyclic voltammogram (CV) of **1**, exhibiting half-wave oxidation potentials of $E_1^{1/2} = +0.70$ and $E_2^{1/2} = +0.91$ V (vs SCE in PhCN at 25°C, scan rate: 500 mV s^{-1}). Thus, the cation radical state and the dication state of **1** appears to be stable in solution.

The first oxidation potential ($E_1^{1/2}$) of **1** is more positive by 0.03 V than that of BETS ($E_1^{1/2} = +0.67$ V vs SCE in PhCN at 25°C, scan rate: 500 mV s^{-1}). This would be ascribed to the stabilization of the energy level of the HOMO by the extension with the dihydrothiophene ring as a linking bridge. The Coulomb repulsive energy is reduced by the extension with the dihydrothiophene ring, since the $\Delta E(= E_2^{1/2} - E_1^{1/2})$ value of **1** (0.21 V) is smaller than that of BETS (0.23 V).

3.2. Electrical conductivities

The conducting properties of the MX_4^- ($MX_4^- = FeCl_4^-$, $GaCl_4^-$, $FeBr_4^-$ and $GaBr_4^-$) salts of BEDT-HBDST are summarized in Table 1. These four salts exhibit semiconductive behavior and the activation energies of them are almost same in the range of temperature from 220 to 300 K. However, there is a great difference between the MCl_4^- and MBr_4^- salts in the conducting

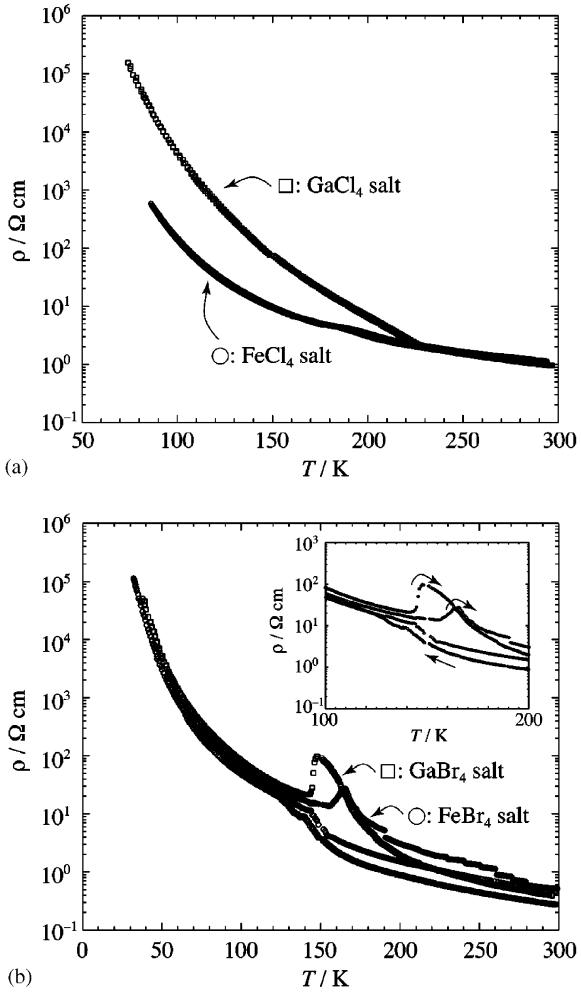

Fig. 1. Temperature dependence of the resistivity of (a) (BEDT-HBDST)$_2MCl_4$ and (b) (BEDT-HBDST)$_2MBr_4$ (M = Fe and Ga). The inset is an expansion in the temperature range from 100 to 200 K.

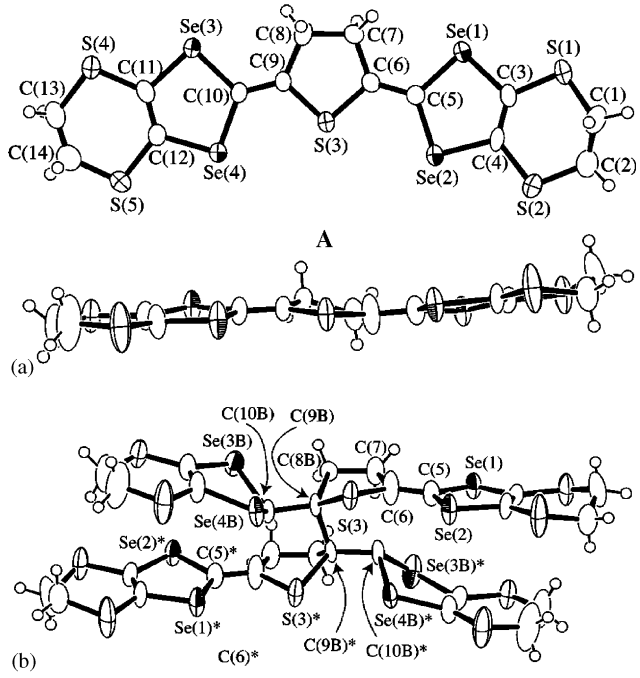

Fig. 2. Molecular structures of the donor molecules of (BEDT-HBDST)$_2FeCl_4$: (a) the major orientation (occupancy: 0.76(1)) and (b) the minor orientation (occupancy: 0.25(1)).

Table 3
Occupancies of the two orientations in (BEDT-HBDST)$_2MX_4$[a]

MX_4^-	Major orientation	Minor orientation
$FeCl_4^-$	0.76(1)	0.25(1)
$GaCl_4^-$	~1	~0
$FeBr_4^-$	0.57(1)	0.43(1)
$GaBr_4^-$	0.56(2)	0.44(2)

[a] The structure of the disordered molecule are depicted in Fig. 2. The occupancies were refined by least-squares method.

properties at low temperature. In the case of the MCl_4^- salts, anomalies in the resistivity were observed at 180 K for the $FeCl_4^-$ salt and at 220 K for the $GaCl_4^-$ salt as shown in Fig. 1(a). On the contrary, hystereses in the resistivity were observed in the temperature range from 140 to 220 K for the MBr_4^- salts as shown in Fig. 1(b).

3.3. Crystal structures

The crystallographic data of the MX_4^- (MX_4^- = $FeCl_4^-$, $GaCl_4^-$, $FeBr_4^-$ and $GaBr_4^-$) salts of BEDT-HBDST are summarized in Table 2. X-ray crystallographic analysis disclosed that these four salts are isostructural with each other. The single crystals of these salts belong to the monoclinic system and the space group of $P2/c$. There is one crystallographically independent donor molecule **A**, adopting fairly good planar conformations as shown in Fig. 2(a). However, the conventional R factors of the X-ray structural analyses of the $FeCl_4^-$, $FeBr_4^-$, and $GaBr_4^-$ salts did not decrease within the allowable value without considering the existence of a disordered donor molecule with partial occupation. The minor disordered molecule is depicted in Fig. 2(b). In the $FeCl_4^-$ salt, the minor orientation is revealed by the division of the Se(3), Se(4), C(8), C(9) and C(10) atoms of the major orientation (**A**) into two positions in the least-squares refinement.[1] In the MBr_4^- (M = Fe and Ga) salts, the minor orientations are revealed by the division of the Se(3), Se(4), C(6), C(8), C(9) and C(10) atoms into two positions.[2] The occupancies of the major and minor orientations are summarized in Table 3. The occupancy of the minor orientation in the $GaCl_4^-$ salt is too small to be detected by the X-ray crystallographic analysis.

[1] The C(9B)–C(9B)* bond length in the minor orientation is 1.70(5) Å for the $FeCl_4^-$ salt. Thus this bond is regarded as a C–C single bond with highly steric repulsion.

[2] The C(9B)–C(9B)*, C(6B)–C(10B)*, and C(10B)–C(6B)* bond lengths in the minor orientation are 1.70(4), 1.51(4), and 1.51(4) Å for the $FeBr_4^-$ salt and 1.59(5), 1.51(4), and 1.51(4) Å for the $GaBr_4^-$ salt. The long C(9B)–C(9B) bond can be ascribed to highly steric repulsion.

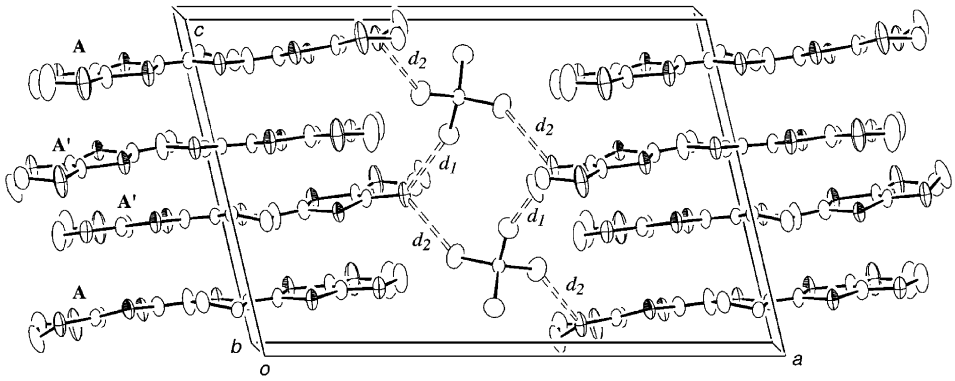

Fig. 3. Crystal structure of (BEDT-HBDST)$_2$FeCl$_4$. The broken lines indicate short S···Cl interactions [$d_1 = 3.634(3)$ and $d_2 = 3.705(4)$ Å]. The minor orientation and hydrogen atoms are omitted for clarity.

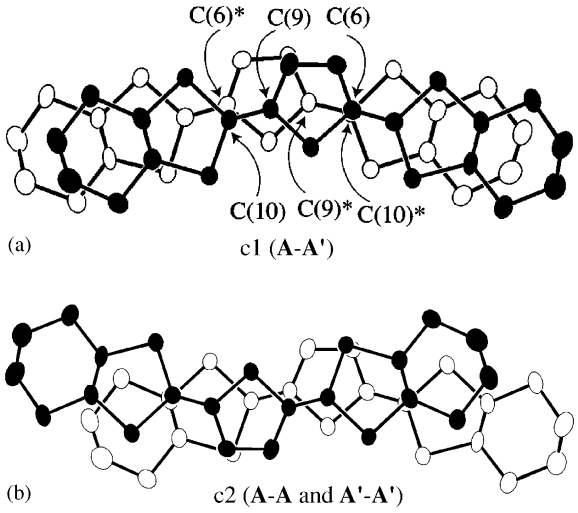

Fig. 4. Overlapping modes of the donor molecules in (BEDT-HBDST)$_2$FeCl$_4$: (a) intra-dimer c1 and (b) inter-dimer c2. The atoms in the front molecule are represented with solid circles and those in the rear molecule are represented with open circles. The minor orientation and hydrogen atoms are omitted for clarity.

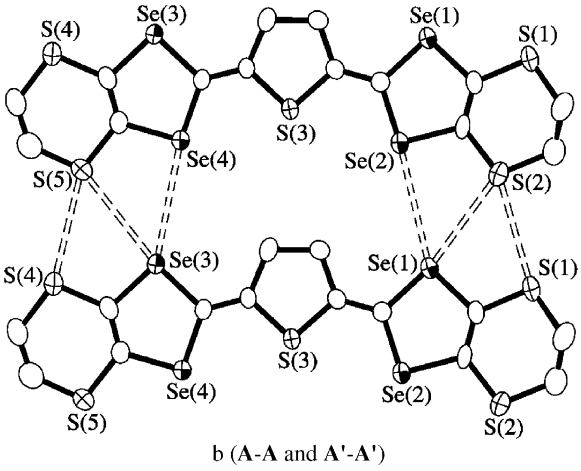

Fig. 5. Side-by-side interaction b (**A**–**A** and **A**′–**A**′) of the donor molecules in (BEDT-HBDST)$_2$FeCl$_4$. The interaction b is shown in Fig. 6. The broken lines indicate short Se···Se, Se···S, and S···S interactions. The minor orientation and hydrogen atoms are omitted for clarity.

In the major orientations of these salts, the donor molecules stack in the –**A**–**A**′–**A**′–**A**– type four-fold period repetition along the *c*-axis as shown in Fig. 3. In consequence, there are two intra-stack intermolecular overlapping modes, c1 (**A**–**A**′) and c2 (**A**–**A** and **A**′–**A**′) as shown in Fig. 4. In the overlapping mode c1, the two donor molecules direct the central sulfur atom to the same side by slipping ca. 1.6 Å along the donor long axis. This overlapping mode is the so-called ring-over-bond type and is quite favorable for a high intermolecular overlapping interaction. In the overlapping modes c2, the two donor molecules direct the central sulfur atom to the opposite side with by slipping ca. 2.9 Å along the donor long axis. The overlapping mode of c2 is quite favorable to avoid the steric repulsion of the central ethylene moiety. However, in these two overlapping modes of c1 and c2, there is no chalcogen–chalcogen atom contact shorter than the van der Waals distances. The overlapping mode of the 1,3-diselenole rings in c2 closely resemble to the twisted overlapping mode in δ'-(BEDT-TTF)$_2$FeCl$_4$ or δ'-(BEDT-TTF)$_2$GaCl$_4$ [14]. As we can see in Fig. 5, the donor molecules are coplanarly linked side-by-side by the short Se···Se, Se···S and S···S contacts shorter than the van der Waals distances. The Se···Se, Se···S and S···S distances are listed in Table 4. Thus, the quasi one-dimensional layered intermolecular π-electron overlapping network is constructed along the *bc*-plane as shown in Fig. 6. The donor arrangement of these salts are analogous to δ-phase BEDT-TTF-based organic conductors [15].

We have determined the crystal structure of the new donor, BEDT-HBDST, itself. There is no disordered molecule in the new donor in the neutral state. The crystal data were deposited as supplementary materials.

Table 4
Intermolecular Se···Se, Se···S and S···S contacts[a] (Å) in (BEDT-HBDST)$_2MX_4$ (MX_4^- = $FeCl_4^-$, $GaCl_4^-$, $FeBr_4^-$ and $GaBr_4^-$)

Interaction	$FeCl_4^-$	$GaCl_4^-$	$FeBr_4^-$	$GaBr_4^-$
Se(1)···Se(2)	3.7546(9)	3.7238(8)	3.800(2)	3.800(2)
Se(3)···Se(4)	3.652(4)	3.6859(8)	3.638(6)	3.77(1)
Se(1)···S(2)	3.526(2)	3.507(2)	3.588(4)	3.590(4)
Se(3)···S(5)	3.481(4)	3.491(2)	3.467(7)	3.59(1)
S(1)···S(2)	3.488(3)	3.467(3)	3.509(5)	3.506(5)
S(4)···S(5)	3.400(2)	3.404(2)	3.414(4)	3.414(4)

[a] The side-by-side interaction b is depicted in Fig. 5. Sum of the van der Waals radii: Se···Se, 3.80; Se···S, 3.70; S···S, 3.60 Å.

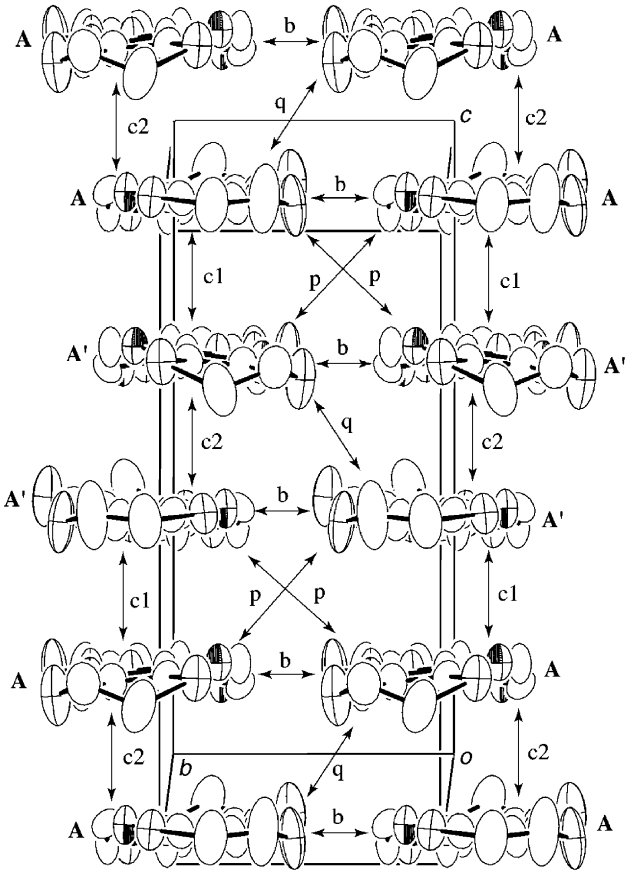

Fig. 6. Molecular arrangement of the donor molecules of (BEDT-HBDST)$_2FeCl_4$ viewed along the donor long axis. The minor orientation and hydrogen atoms are omitted for clarity. The donor arrangement of the other salts are essentially the same as that shown here.

3.4. Band structures

The intermolecular overlap integrals of the four salts, (BEDT-HBDST)$_2MX_4$ (MX_4^- = $FeCl_4^-$, $GaCl_4^-$, $FeBr_4^-$ and $GaBr_4^-$), were calculated based on the crystal structure obtained by the X-ray analysis. To clarify the effect of the disorder of the donor molecules, we have calculated the overlap integrals on the two orientations which are summarized in Table 5. The 'divided' means the calculation on the major orientation. On the other hand, the 'disorder' means the calculation on the disordered configuration, in which the disordered groups were not divided.[3] In either case, the symmetry of the π-AO coefficients in the HOMOs are not different from each other, namely, all the S and Se atoms have the same phase, and all the sp^2 carbon atoms have the reverse phase. As shown in Table 5, the intra-dimer overlap integrals (c1) of these salts are significantly large, since the overlapping mode of c1 is quite favorable for giving a high intermolecular HOMO–HOMO bonding interaction due to the so-called ring-over-bond type overlapping. On the contrary, the inter-dimer overlap integrals c2 of them are less than c1. The ratio of the calculated overlap integrals (c2/c1) is 0.60–0.77 in the case of the divided orientation. On the other hand, the ratio of overlap integrals (c2/c1) is 0.32–0.46 in the case of the disorder orientation. As the occupancy of the minor orientation increases, the degree of dimerization tends to become stronger.

Using the overlap integrals listed in Table 5, the band structures and the Fermi surfaces of the $FeCl_4^-$ and $FeBr_4^-$ salts were calculated by the tight-binding approximation method and depicted in Figs. 7(a), (c) and (b), (d), respectively. When the band calculations were carried out by using the overlap integrals of the disorder orientation, there is a midgap between the upper two bands and the lower two bands (Figs. 7(a) and (b)), which is ascribed to the dimerization of the donor molecules. In this case, the upper two bands are effectively half-filled, since the composition of D:A = 2:1. When the band calculations were carried out by using the overlap integrals of the divided orientation, the energy bands have a quarter-filled band structure (Figs. 7(c) and (d)). The semiconducting behavior of the $FeCl_4^-$ and $FeBr_4^-$ salts can be mainly ascribed to the disorder of the donor molecules, since the disordered salts having one-dimensional character and having the half-filled upper band structure are liable to become Mott-type insulators.

[3] In the least-squares refinement, the disordered groups were not divided and the refinement has converged. Atomic coordinates used for the calculation of overlap integrals of 'disorder' are available as supplementary data.

Table 5
Calculated overlap integrals[a] S ($\times 10^{-3}$) in (BEDT-HBDST)$_2MX_4$ (MX_4^- = $FeCl_4^-$, $GaCl_4^-$, $FeBr_4^-$ and $GaBr_4^-$)

Interaction			$FeCl_4^-$		$GaCl_4^-$	$FeBr_4^-$		$GaBr_4^-$	
			Disorder	Divided		Disorder	Divided	Disorder	Divided
Intra-column	Intra-dimer	c1	26.93	23.85	25.65	32.83	21.19	31.52	19.77
	Inter-dimer	c2	12.32	14.35	13.07	10.91	15.89	10.23	15.18
Inter-column	Transverse	b	7.98	8.06	7.44	7.08	6.91	6.92	7.55
	Oblique	p	1.62	1.61	1.42	2.44	1.26	2.30	1.37
		q	2.22	3.56	3.20	2.02	3.25	2.03	3.30
Ratio (c2/c1)			0.46	0.60	0.51	0.33	0.75	0.32	0.77

[a] The interaction types of c1, c2, b, p and q are indicated in Fig. 6.

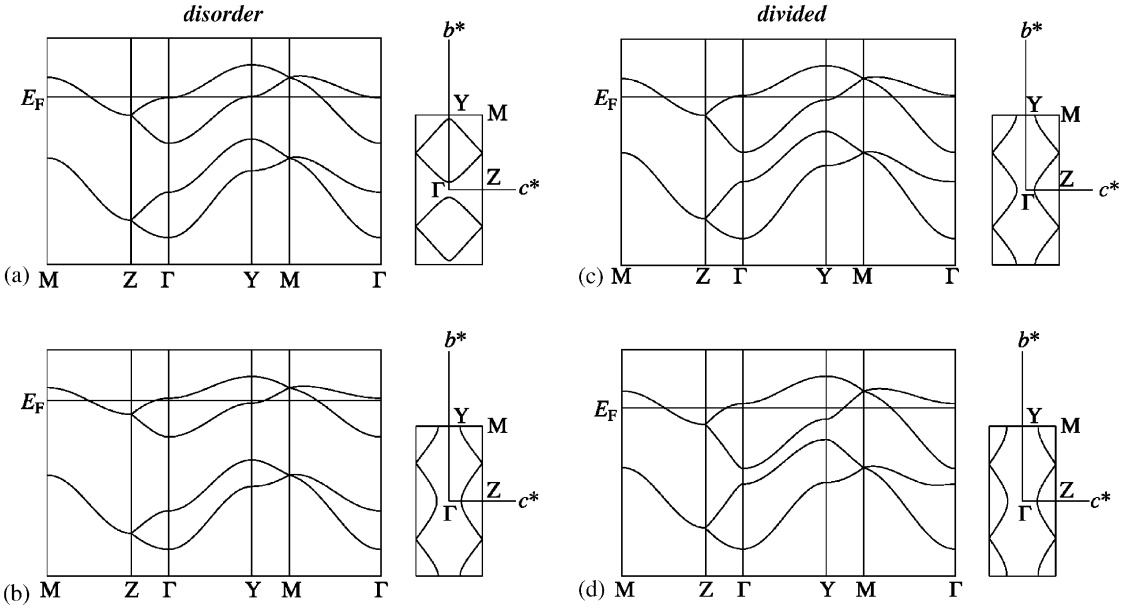

Fig. 7. Calculated energy band dispersions and Fermi surfaces of (a, c): (BEDT-HDBST)$_2FeCl_4$ and (b, d): (BEDT-HBDST)$_2FeBr_4$. The calculations were carried out based on (a, b) the overlap integrals of 'disorder' and on (c, d) the overlap integrals of 'divided' listed in Table 5.

3.5. Magnetic properties

Temperature dependence of the magnetic susceptibilities of (BEDT-HBDST)$_2FeX_4$ (X = Cl and Br), as well as the reference compound, (BEDT-HBDST)$_2GaCl_4$, was measured down to 2 or 5 K by using a SQUID magnetometer. The magnetic susceptibility of the non-magnetic anion salt, (BEDT-HBDST)$_2GaCl_4$, where the susceptibility is attributed to the donor π-system only, monotonically increased with decrease in temperature as shown in Fig. 8. The magnetic behavior of the $GaCl_4^-$ salt fitted to Curie–Weiss law with the Curie constant of $C = 0.38\,\text{emu K mol}^{-1}$ and with the Weiss temperature of $\theta = -1.2\,\text{K}$. The Curie constant of $C = 0.38\,\text{emu K mol}^{-1}$ agree with the case of the one spin of $S = 1/2$ per formula unit, because the calculated value of $0.37\,\text{emu K mol}^{-1}$, using $[N_A \cdot g^2 \cdot \mu_B^2 \cdot S \cdot (S+1)/(3k_B)]$ for an $S = 1/2$ localized spin system with $g = 2.0$, is very close to the obtained value of the Curie constant.

As shown in Figs. 9(a) and (b), the susceptibility of the $FeCl_4^-$ salt follows the Curie–Weiss law with the Curie constant of $C = 4.6\,\text{emu K mol}^{-1}$ and with the Weiss temperature of $\theta = -1.2\,\text{K}$. The Curie constant of $C = 4.6\,\text{emu K mol}^{-1}$ indicates a high spin-state of $S = 5/2$ for the Fe^{3+} ion, because the sum of the calculated values of 4.38 ($S = 5/2$) and 0.37 ($S = 1/2$) emu K mol^{-1} is very close to the obtained value of the Curie constant. A weak antiferromagnetic interaction between the 3d spins in the $FeCl_4^-$ salt is revealed from the small value of $\theta = -1.2\,\text{K}$. As shown in Figs. 9(a) and (b), the experimentally measured magnetization is well fitted to the solid line calculated by using Brillouin function with the parameters of S ($=J$) = 5/2 and $\theta = -1.2\,\text{K}$ for $T^* = T - \theta$. The S···Cl, S···Br, Fe···Fe, Cl···Cl and Br···Br distances, as well as the Weiss temperature are summarized in Table 6. Although there is no short Se···Cl contact, there are short S···Cl contacts ($d_1 = 3.634(3)$ and

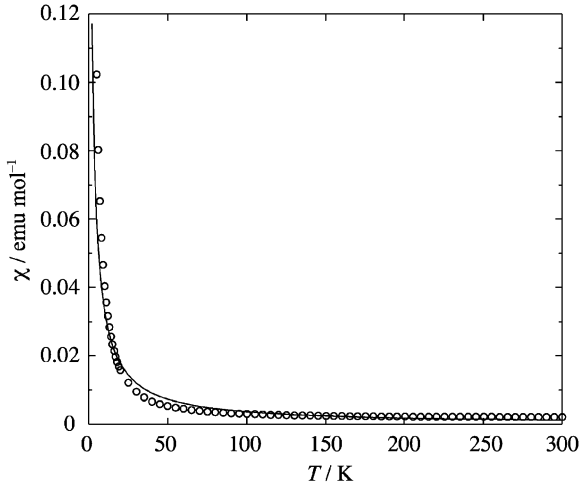

Fig. 8. Temperature dependence of the magnetic susceptibility of $(BEDT\text{-}HDBST)_2GaCl_4$ with an applied field of 9.0 kOe. The solid line is calculated by Curie–Weiss law with $C = 0.38$ emu K mol^{-1} and $\theta = -1.2$ K.

$d_2 = 3.705(4)$ Å) as shown in Fig. 3. In addition, the shortest Cl···Cl (4.810(4) Å) distance of the $FeCl_4^-$ salt is far longer than the van der Waals distance (Cl···Cl = 3.50 Å). The shortest Fe···Fe distance (6.6586(5) Å) of the $FeCl_4^-$ salt is longer by 0.779 Å than that of κ-$(BETS)_2FeCl_4$ (5.879 Å), on which a π–d interaction has been observed quite recently [6]. The Fe···Fe and Cl···Cl distances of $(BEDT\text{-}HBDST)_2FeCl_4$ appear to be too long to permit the direct magnetic interaction between the 3d spins of the nearest neighboring Fe^{3+} ions. To estimate the extent of the π–d interaction and the extent of the direct d–d interaction of the $FeCl_4^-$ salt, magnetic interactions $J_{\pi d}$ and J_{dd} are evaluated by using the equation $J = -2t^2/U$ (t: transfer integral and U: Coulomb integral) based on the calculated π–d and d–d overlap integrals obtained by the extended Hückel MO calculations [17]. The largest $J_{\pi d}$ (–1.69 K) and the largest J_{dd} (–0.020 K) of the $FeCl_4^-$ salt are nearly same as those of κ-$(BETS)_2FeCl_4$ ($J_{\pi d} = -1.22$ K and $J_{dd} = -0.0205$ K). This fact suggests that $(BEDT\text{-}HBDST)_2FeCl_4$ may have an antiferromagnetic ground state at low temperature similar to that of κ-$(BETS)_2FeCl_4$ (0.65 K). However, further investigation should be continued to prove the existence of the π-mediated antiferromagnetic ground state since the Weiss temperature is small.

The magnetic susceptibility of $(BEDT\text{-}HBDST)_2FeBr_4$ also follows the Curie–Weiss law with the Curie constant of $C = 4.8$ emu K mol^{-1} and the Weiss temperature of $\theta = -4.9$ K as shown in Fig. 10. Thus, it is indicated that the Fe^{3+} ions of the $FeBr_4^-$ salt exist in the high-spin state of $S = 5/2$ and the spin of $S = 1/2$ is contributed from the π-system of the donor molecule. The antiferromagnetic interaction between the 3d spins of the Fe^{3+} ions of the $FeBr_4^-$ salt is stronger than that

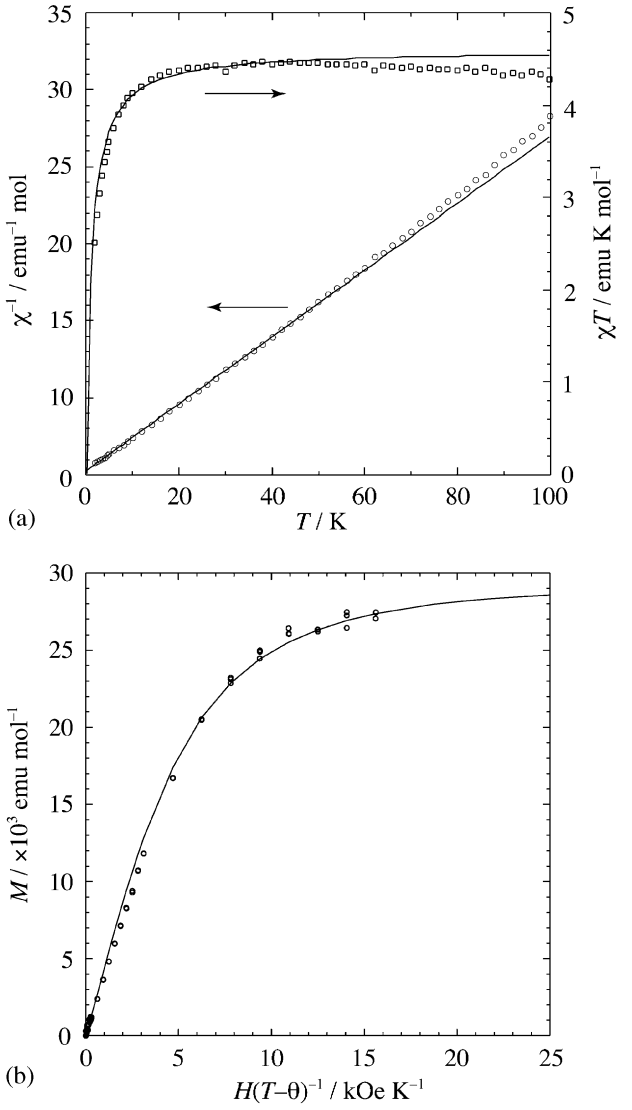

Fig. 9. Magnetic property of $(BEDT\text{-}HBDST)_2FeCl_4$: (a) $\chi^{-1}-T$ and $\chi T-T$ plots of $(BEDT\text{-}HBDST)_2FeCl_4$ with an applied field of 1.0 kOe. The solid lines are calculated by Curie–Weiss law with $C = 4.6$ emu K mol^{-1} and $\theta = -1.2$ K. (b) Magnetization as a function of $H/(T-\theta)$ for $(BEDT\text{-}HBDST)_2FeCl_4$ at 2 K. The solid line is calculated by Brillouin function with the parameters of $S\ (=J) = 5/2$ and $\theta = -1.2$ K for $T^* = T-\theta$.

of the $FeCl_4^-$ salt. Indeed, there are two S···Br contacts ($d_3 = 3.681(4)$ and $d_4 = 3.734(5)$ Å). On the contrary, the shortest Br···Br distance (4.744(3) Å) of the $FeBr_4^-$ salt is far longer than the van der Waals distance (Br···Br = 3.70 Å) and the shortest Fe···Fe distance (6.6722(8) Å) is longer by 0.752 Å than that of κ-$(BETS)_2FeBr_4$ (5.920 Å). Judging from the fairly long Fe···Fe and Br···Br distances, the direct magnetic interaction between the 3d spins of the nearest neighboring Fe^{3+} ions appears to be not so easy to occur. However, further investigation is also necessary to clarify the mechanism of the magnetic interactions in $(BEDT\text{-}HBDST)_2FeBr_4$.

Table 6
Nearest inter-atom distances (Å) and θ (K) values of $FeCl_4^-$ and $FeBr_4^-$ salts of BEDT-HBDST compared with BETS salts[a]

Compound	Donor–anion	Anion–anion		θ(K)
	S···Cl (S···Br)	Fe···Fe	Cl···Cl (Br···Br)	
$(BEDT\text{-}HBDST)_2FeCl_4$	3.634(3)	6.6586(5)	4.810(4)	−1.2
	3.705(4)	7.5636(1)	4.819(3)	
$(BEDT\text{-}HBDST)_2FeBr_4$	3.681(4)	6.6722(8)	4.744(3)	−4.9
	3.734(5)	7.5998(1)	4.768(3)	
κ-$(BETS)_2FeCl_4$	3.547	5.879	4.12	−0.8
	3.592			
κ-$(BETS)_2FeBr_4$	3.693	5.920	4.137	−5.5
	3.776			

[a] The inter-atom distance and Weiss temperature of κ-$(BETS)_2FeX_4$ were taken from the Refs. [6] and [16], respectively.

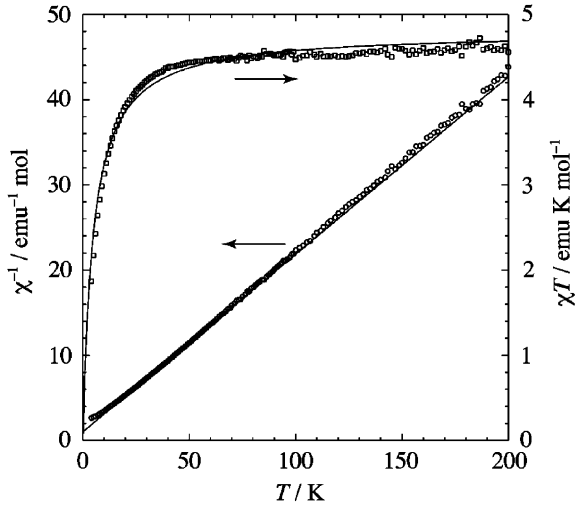

Fig. 10. $\chi^{-1}-T$ and $\chi T-T$ plots of $(BEDT\text{-}HBDST)_2FeBr_4$ with an applied field of 1.0 kOe. The solid lines are calculated by Curie–Weiss law with $C = 4.8$ emu K mol^{-1} and $\theta = -4.9$ K.

4. Conclusion

A novel π-extended BETS-type donor, BEDT-HBDST was synthesized by a convenient method. The first oxidation potential of BEDT-HBDST ($E_1^{1/2} = +0.70$ V vs. SCE) is more positive by 0.03 V than that of BETS ($E_1^{1/2} = +0.67$ V vs. SCE). BEDT-HBDST based four cation radical salts with magnetic and non-magnetic anions, $(BEDT\text{-}HBDST)_2MX_4$ (MX_4^- = $FeCl_4^-$, $GaCl_4^-$, $FeBr_4^-$ and $GaBr_4^-$), showing semiconducting behavior were prepared. The donor molecules of $FeCl_4^-$, $FeBr_4^-$ and $GaBr_4^-$ salts are disordered containing a disordered molecule as a minor orientation. In the major orientation, the donor molecules stack in the four-fold period of repetition, and the degree of dimerization is fairly strong in the stacking direction. The donor layers of these salts are parallel to the *bc*-plane. The origin of the semiconducting behavior of these salts can be ascribed to the disorder of the donor molecules, since the energy bands calculated on the major orientations are quarter-filled band structure, whereas the energy bands calculated on the disordered orientations are half-filled band structure in the upper two bands. The magnetic $FeCl_4^-$ and $FeBr_4^-$ salts exhibited Curie–Weiss behavior with negative Weiss temperatures of $\theta = -1.2$ and -4.9 K, respectively. There are several short S···Cl and S···Br contacts in the crystal structures. Moreover, the shortest Fe···Fe and Cl···Cl as well as Br···Br distances appear to be too long to permit the direct magnetic interaction between the 3d spins of the nearest neighboring Fe^{3+} ions. However, more detailed studies are needed to clarify the mechanism of the antiferromagnetic interactions of the 3d spins of the Fe^{3+} ions of the FeX_4^- (X = Cl and Br) salts.

Acknowledgments

The authors acknowledge Prof. Y. Nozue of Physics Department of Graduate School of Science, Tohoku University and Prof. T. Nojima of Center for Low Temperature Science, Tohoku University for allowing the use of their SQUID magnetometer. We thank Dr. S. Endo of Center for Low Temperature Science, Tohoku University for the kind assistance in using the SQUID magnetometer. We are also grateful to Dr. T. Imakubo of the Institute of Physical and Chemical Research (RIKEN) for his useful comments of crystal structure analyses.

References

[1] P. Batail, L. Ouahab, J.B. Torrance, M.L. Pylman, S.S.P. Parkin, Solid State Commun. 55 (1985) 597.
[2] R. Kato, Bull. Chem. Soc. Jpn. 73 (2000) 515;
H. Kobayashi, A. Miyamoto, R. Kato, F. Sakai, A. Kobayashi, Y. Yamakita, Y. Furukawa, M. Tasumi, T. Watanabe, Phys. Rev. B 45 (1993) 3500;
H. Kobayashi, H. Sawa, S. Aonuma, R. Kato, J. Am. Chem. Soc. 115 (1993) 7870.

[3] L.I. Buravov, A.V. Gudenko, V.B. Ginodman, A.V. Zvarykina, V.E. Korotkov, N.D. Kushch, L.P. Rozenberg, A.G. Khomenko, R.P. Shibaeva, E.B. Yagubskii, Izv. Akad. Nauk SSSP, Ser, Kim., N1 (1990) 206;
P. Day, M. Kumoo, T. Mallah, I.R. Marsden, R.H. Friend, F.L. Pratt, W. Hayes, D. Chasseau, J. Gautier, G. Bravic, L. Ducasse, J. Am. Chem. Soc. 114 (1992) 10722.

[4] P. Day, C. R. Acad. Sci. Ser., IIc: Chim. 2 (1999) 675; A.W. Graham. M. Kurmoo, P. Day, Chem. Commun. 2061 (1995);
M. Kurmoo, A.W. Graham, P. Day, S.J. Coles, M.B. Hursthouse, J.L. Caulfield, J. Singleton, F.L. Pratt, W. Hayes, L. Ducasse, P. Guionneau, J. Am. Chem. Soc. 117 (1995) 12209.

[5] H. Kobayashi, H. Tomita, T. Naito, A. Kobayashi, F. Sasaki, T. Watanabe, P. Cassoux, J. Am. Chem. Soc. 118 (1996) 368;
H. Kobayashi, A. Kobayashi, P. Cassoux, Chem. Soc. Rev. 29 (2000) 325.

[6] H. Fujiwara, E. Fujiwara, Y. Nakazawa, B.Zh. Narymbetov, K. Kato, H. Kobayashi, A. Kobayashi, M. Tokumoto, P. Cassoux, J. Am. Chem. Soc. 123 (2001) 306; T. Otsuka, A. Kobayashi, Y. Miyamoto, J. Kiuchi, N. Wada, E. Ojima, H. Fujiwara, H. Kobayashi, Chem. Lett. (2000) 732;
T. Otsuka, A. Kobayashi, Y. Miyamoto, J. Kikuchi, S. Nakamura, N. Wada, E. Fujiwara, H. Fujiwara, H. Kobayashi, J. Solid State Chem. 159 (2001) 407.

[7] T. Ise, T. Mori, K. Takahashi, Chem. Lett. (1997) 1031;
T. Ise, T. Mori, K. Takahashi, J. Mater. Chem. 11 (2001) 264;
K. Takahashi, T. Shirahata, K. Tomitani, J. Mater. Chem. 7 (1997) 2375;
K. Takahashi, T. Shirahata, Chem. Lett. (2001) 514;
K. Imaeda, Y. Yamashita, S. Tanaka, H. Inokuchi, Synth. Met. 73 (1995) 107;
Y. Yamashita, M. Tomura, J. Mater. Chem. 8 (1998) 1933;
M.R. Bryce, J. Chem. Soc., Parkin Trans. 1 (1985) 1675;
P. Frère, K. Boubekeur, M. Jubault, P. Batail, A. Gorgues, Eur. J. Org. Chem. (2001) 3741;
Y. Misaki, N. Higuchi, H. Fujiwara, T. Yamabe, T. Mori, H. Mori, S. Tanaka, Angew. Chem. Int. Ed. Engl. 34 (1995) 1222.

[8] H.J. Jacobsen, E.H. Larsen, S.-O. Lawesson, Tetrahedron 19 (1936) 1867.

[9] R. Kato, H. Kobayashi, A. Kobayashi, Synth. Met. 42 (1991) 2093; T. Courcet, I. Malfant, K. Pokhodnia, P. Cassoux, New J. Chem. (1998) 585.

[10] G.M. Sheldrick, SADABS, Empirical Absorption Correction Program, University of Göttingen, Germany, 1997.

[11] G.M. Sheldrick, SHELX-97, A Computer Program for Refinement of Crystal Structures, University of Göttingen, Germany, 1997.

[12] R. Hoffman, J. Phys. Chem. 39 (1963) 1397.

[13] T. Mori, A. Kobayashi, Y. Sasaki, H. Kobayashi, G. Saito, H. Inokuchi, Bull. Chem. Soc. Jpn. 57 (1984) 627;
M.-H. Whangbo, J.M. Williams, P.C.W. Leung, M.A. Beno, T.J. Emge, H.H. Wang, K.D. Carlson, G.W. Crabtree, J. Am. Chem. Soc. 107 (1985) 5815.

[14] T. Mallah, C. Hollis, S. Bott, M. Kurmoo, P. Day, M. Allan, R.H. Friend, J. Chem. Soc., Dalton Trans. (1990) 859;
M. Allan, R.H. Friend, D. Chasseau, G. Bravic, P. Day, Synth. Mett. 42 (1991) 2127;
M. Kurmoo, P. Day, P. Guionneau, G. Bravic, D. Chasseau, L. Ducasse, M.L. Allan, I.D. Marsden, R.H. Friend, Inorg. Chem. 35 (1996) 4719.

[15] T. Mori, Bull. Chem. Soc. Jpn. 72 (1999) 2011.

[16] H. Uozaki, K. Okamoto, S. Endo, H. Matsui, K. Ueda, T. Sugimoto, N. Toyota, Synth. Met. 103 (1999) 1984;
H. Uozaki, T. Sasaki, S. Endo, N. Toyota, J. Phys. Soc. Jpn. 69 (2000) 2759.

[17] T. Mori, M. Katsuhara, J. Phys. Soc. Jpn. 71 (2002) 826.